AIP | APL Materials

Research Update: Nanoscale surface potential analysis of MoS2 field-effect transistors for biomolecular detection using Kelvin probe force microscopy

Min Hyung Kim, Heekyeong Park, Hyungbeen Lee, Kihwan Nam, Seokhwan Jeong, Inturu Omkaram, Dae Sung Yoon, Sei Young Lee, Sunkook Kim, and Sang Woo Lee

Citation: APL Mater. **4**, 100701 (2016); doi: 10.1063/1.4964488
View online: http://dx.doi.org/10.1063/1.4964488
View Table of Contents: http://scitation.aip.org/content/aip/journal/aplmater/4/10?ver=pdfcov
Published by the AIP Publishing

Research Update: Nanoscale surface potential analysis of MoS_2 field-effect transistors for biomolecular detection using Kelvin probe force microscopy

Min Hyung Kim,[1,a] Heekyeong Park,[2,a] Hyungbeen Lee,[1,a] Kihwan Nam,[3] Seokhwan Jeong,[2] Inturu Omkaram,[2] Dae Sung Yoon,[4] Sei Young Lee,[1,b] Sunkook Kim,[2,b] and Sang Woo Lee[1,b]

[1]*Department of Biomedical Engineering, Yonsei University, Wonju 26493, South Korea*
[2]*Multi-Functional Nano/Bio Electronics Laboratory, Kyung Hee University, Gyeonggi 446-701, South Korea*
[3]*Center for Bionics, Biomedical Research Institute, Korea Institute of Science and Technology, Seoul 02792, South Korea*
[4]*Department of Bio-convergence Engineering, Korea University, Seoul 136-701, South Korea*

(Received 6 July 2016; accepted 29 August 2016; published online 10 October 2016)

We used high-resolution Kelvin probe force microscopy (KPFM) to investigate the immobilization of a prostate specific antigen (PSA) antibody by measuring the surface potential (SP) on a MoS_2 surface over an extensive concentration range (1 pg/ml–100 μg/ml). After PSA antibody immobilization, we demonstrated that the SP on the MoS_2 surface characterized by KPFM strongly correlated to the electrical signal of a MoS_2 bioFET. This demonstration can not only be used to optimize the immobilization conditions for captured molecules, but can also be applied as a diagnostic tool to complement the electrical detection of a MoS_2 FET biosensor. [http://dx.doi.org/10.1063/1.4964488]

Label-free sensing methods for the detection of biomolecules have been intensively researched in various applications because of their simplicity, convenience, and non-interference.[1–5] Among these label-free sensing methods, electrical detection methods using one-dimensional (1D) field-effect transistor (FET) devices composed of carbon nanotubes,[6–8] silicon nanowires,[9,10] and conducting polymer nanowires[11,12] have gradually increased during the past few years because their sensing parameters, such as threshold voltage, mobility, and "OFF-current," provide exquisite sensitivity and high-throughput analysis. The large surface-to-volume ratio and Debye length in these 1D nano-scaled semiconducting biosensors also allow detection of a small number of biomolecules on the biosensor surface. Even a few biomolecules dramatically change the surface charge carrier density or surface potential (SP) of the device, resulting in much higher sensitivity than is available with other detection devices.[13–16] However, 1D semiconductor biosensors still have limitations such as device-to-device performance variation, non-uniformity, and a small integration area.[17,18]

2D layered semiconductor-based sensors with a high surface-to-volume ratio have fewer limitations than 1D semiconductor biosensors. 2D devices offer highly sensitive detection for biomolecules and ions and serve as the basis for conventional planar devices in large-area integration.[19,20] Specifically, molybdenum disulfide (MoS_2), which is the most investigated 2D material in the transition metal dichalcogenide family, is a promising candidate for applications in sensing devices.[21,22] Recent reports demonstrated that MoS_2-based FETs could be candidates for biological sensors

[a]M. H. Kim, H. Park, and H. Lee contributed equally to this work.
[b]Authors to whom correspondence should be addressed. Electronic addresses: syl235@yonsei.ac.kr, kimskcnt@gmail.com, and yusuklee@yonsei.ac.kr

and excellent pH sensing alternatives.[23,24] In most cases, a biological sensing element selectively recognizes a particular biological molecule through a reaction, specific adsorption, or other physical or chemical processes, and then the 2D MoS_2 FET converts this recognition into a usable electrical signal. Recently, Lee *et al.* reported that MoS_2 FETs offer a highly hydrophobic MoS_2 surface (water contact angle ~75.77°) without any other post-processing and they also show a high affinity to prostate specific antigen (PSA) antibody (hydrophobic biomolecule).[17] PSA antibodies adsorbed on the MoS_2 surface yield SP variations on the FET surface, resulting in varying I-V characteristics. However, the correlation between the amount of adsorbed PSA antibody and electrical performance remains unclear. Furthermore, to the best of our knowledge, no relevant studies have been performed even though a quantitative analysis of the SP generated by the adsorbed biomolecules is important to designing and optimizing 2D MoS_2 FET-based biosensors.

Kelvin probe force microscopy (KPFM),[25,26] an important technique for investigating surface charges by measuring SP, can measure the charges of a bimolecular functionalized surface on a substrate, thereby identifying the charge state of the adsorbates, the spatial distribution of the charge carriers, and the SP of semiconductors[27] such as graphene,[28,29] carbon nanotubes,[28,30] and silicon nanowire.[31] However, no reports yet describe the correlations among the physically adsorbed biomolecules on the MoS_2 surface of a MoS_2 bioFET or the resultant electrical performance. In this work, we have used KPFM to explore the variation of SP generated by adsorbed PSA antibodies on a 2D MoS_2 bioFET biosensor. We also imaged the surface topology and uniformity to confirm the proper absorption of biomolecules during SP measurement. Furthermore, the variation of the drain-current in the MoS_2 bioFET was measured in the same experimental environment. The relationship between the drain-current and the SP caused by PSA antibody-MoS_2 surface adsorption was examined by comparing those measurement results. This investigation can be useful for designing and optimizing a label-free 2D FET-based biosensor.

We first exfoliated thin-film MoS_2 flakes from bulk MoS_2 using cellophane tape and then transferred the flakes with a thickness in the range of 30–100 nm onto a p-doped Si substrate (the average thickness of 20 different thin-film MoS_2 flake samples ~42 nm ± 10 nm) with SiO_2 (300 nm) as the gate insulator. To clean the wafers and remove residues from the substrates, we placed the MoS_2 flakes on the Si wafer into acetone for 2 hours and sequentially isopropyl alcohol for 10 min. E-beam deposited Ti/Au (20 nm/300 nm) electrodes on the wafers formed the source and drain. Finally, the wafers were annealed in a vacuum tube at 200 °C with H_2 gas (10 SCCM) and Ar gas (100 SCCM) to improve the interface solidarity between the Au and MoS_2 and remove organic residues. The PSA antibody (in phosphate-buffered saline [PBS], pH 7.2) was incubated on the MoS_2 surface of the biosensor for 30 min inside a humidity chamber to prevent evaporation. The sensor was washed in PBS buffer for 1 min to remove weakly bound biomolecules. Three Au-probe tips, including a manipulator for measuring the electrical characteristics, were connected to the source, drain, and gate of the MoS_2 bioFET. Electrical characteristics were evaluated with I-V measurements (Model 4200-SCA Semiconductor Characterization System, Keithley Instrument, Inc., OH, USA). In this experiment, we used five PSA antibody concentrations from 1 pg/ml to 100 μg/ml to measure the currents produced by the MoS_2 biosensor.

After carrying out the procedures just described on the MoS_2 surface, we measured the surface topology and potential using atomic force spectroscopy (AFM) (MultimodeV, Veeco, CA, USA) as follows: we mounted a conducting cantilever tip (SCM-PIT, Bruker, rectangular, platinum-iridium coated, CA, USA) in a tip holder (MMEFCH, Veeco, CA, USA) able to control the tip voltage, where the functional resonance frequency and drive amplitude of the tip are between 60 and 75 kHz, and 1V, respectively. The SP measurements were performed in a lift-mode KPFM. The SP mapping images by KPFM (scan size: 1 μm × 1 μm) were obtained at the scan speed of 1 μm/s, a lift scan height of 33.03 nm, and a drive amplitude voltage of 1–1.5 V, where the temperature was maintained at room temperature.

The aim of our experimental procedure was to analyze the nanoscale SP upon PSA antibody binding to a MoS_2 FET biosensor, as shown in Figure 1. The PSA antibody was physically adsorbed on the MoS_2 surface (i.e., non-specific binding), and then PSA was selectively bound to the physisorbed PSA antibody (Fig. 1(a)), indicating that MoS_2 nanosheet–based PSA detection is a classic label-free immunoassay. Figure 1(b) illustrates an electrical measurement method that

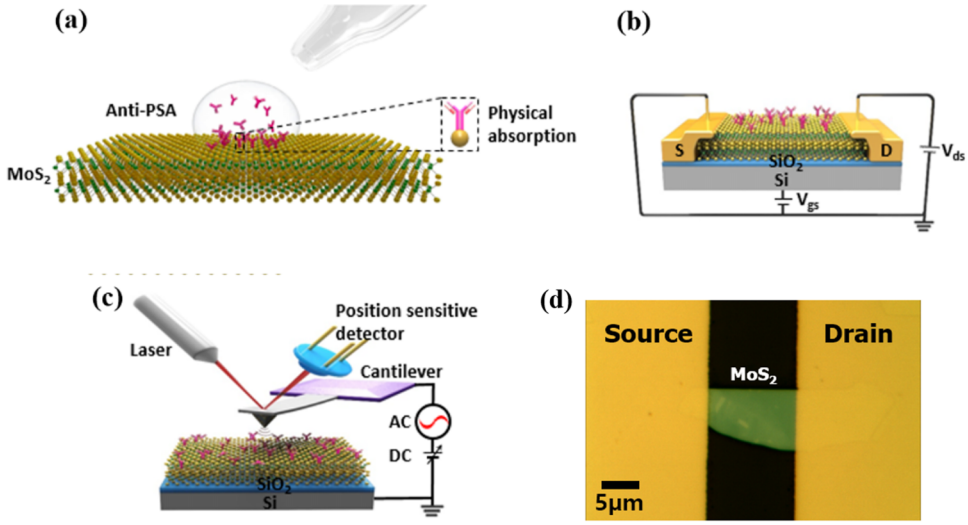

FIG. 1. Schematic illustrations of the measurement system: (a) Anti-PSA binding process on the MoS_2 surface. The hydrophobicity of MoS_2 enables physical adsorption of biomolecules without additional dielectric layers. (b) Electrical measurement method of the bioFET. Physically adsorbed biomolecules cause the gating effect, which can induce a variation of the drain current with respect to the concentration of PSA antibodies. (c) SP characterization by KPFM to identify the charge state of the adsorbates and optimize the immobilization condition. (d) The optical image of the MoS_2 device on Si substrate.

uses the variation in the MoS_2 FET biosensor current upon the change of conductance that occurs when a charged molecule adheres to the MoS_2 sheet surface. The bioFET detection method has several advantages, such as label-free detection, easy preparation, and rapid detection. However, the bioFET method cannot detect at the single-molecule level, which is an important issue when trying to improve the accuracy of a detection technique. In particular, MoS_2 bioFET demands verification of sensor accuracy because the PSA antibody is physically adsorbed on the MoS_2 surface. This technique has often suffered from optimization issues caused by the immobilization of the PSA antibody. To address those issues, we applied high-resolution KPFM to optimize the immobilized quantity of the PSA antibody by measuring the SP on the MoS_2 bioFET over an extensive PSA antibody concentration range (Figure 1(c)).

After PSA antibody immobilization, the SP of the PSA antibody on the MoS_2 bioFET (as characterized by KPFM) correlated with the electrical sensor response of the MoS_2 bioFET. For precise measurement from the KPFM, we optimized the lift scan height and scan speed of the conductive cantilever tip on the KPFM based on previous work.[32–35] We measured both the high-resolution topology and SP images, as shown in Figure 2. Figures 2(c), 2(e), and 2(g) depict representative 3D topology and SP images of the bare MoS_2 surface. From those images, we found that the bare MoS_2 surface has an extremely low surface and SP roughness (Ra < 0.1 nm, 1 mV). In other words, the MoS_2 surface is atomically flat. That information is important[36] because the underlying quality of the substrate, in terms of surface roughness, subsurface damage, and impurity content, critically affects the threshold and component lifetime. To find the optimal conditions for imaging a single PSA antibody, we used KPFM to obtain the height and SP maps of a PSA antibody on the MoS_2 bioFET surface. In Figures 2(d), 2(f), and 2(h), an individual PSA antibody is imaged as a green dot with a height of less than 3 nm, which is consistent with previous studies.[37] Despite the low concentration (1 pg/ml), the PSA antibody is clearly shown in the height and SP images. In an SP map of a PSA antibody on the MoS_2 bioFET, the antibody has positive SP (~200 mV) due to the relatively low work function of MoS_2. It should be noted that the SP of the MoS_2 films used in this experiment might be varied because of the thickness variation of the MoS_2 films. However, as you see in Figure 2(f), the SP of a pristine MoS_2 film is extremely lower than the one of the PSA antibody adsorbed region (e.g., greater than 200 times). Hence, the SP variation due to the thickness variation of the MoS_2 film can be ignored.

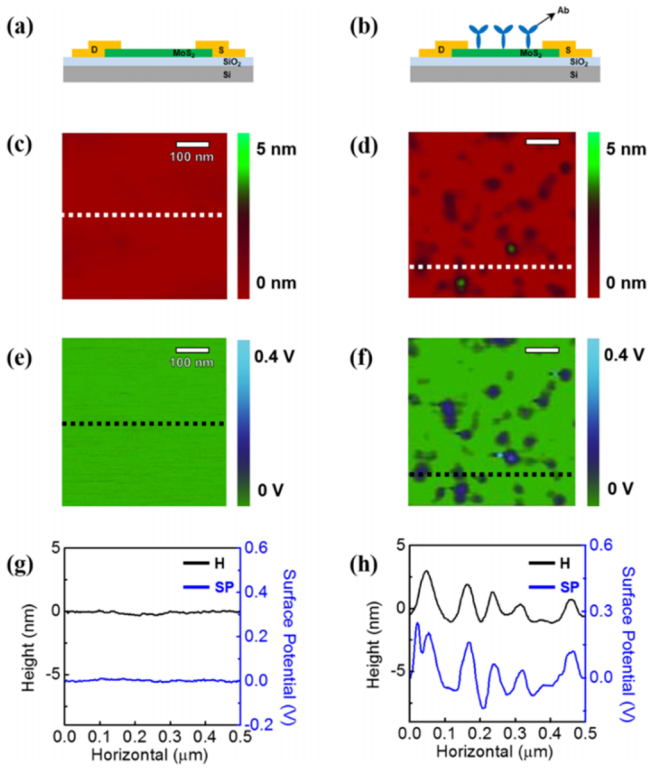

FIG. 2. ((a) and (b)) Schematic representation of (a) the MoS_2 device, and (b) PSA antibodies adsorbed on the MoS_2 bioFET device. ((c) and (d)) Height map images observed by tapping mode AFM: (c) the bare surface of the MoS_2 bioFET device, and (d) PSA antibodies adsorbed on the MoS_2 FET device. ((e) and (f)) SP map images probed by KPFM: (e) the bare surface of the MoS_2 bioFET device, and (f) PSA antibodies adsorbed on the bioFET device. The white or black dotted lines in images ((c)–(f)) represent the trajectory of the line scan for the following cross-sectional views. ((g) and (h)) The corresponding cross-sectional views taken through the height map images and SP map images from ((c)–(f)): (g) the bare surface of the MoS_2 bioFET device, and (h) PSA antibodies adsorbed on the MoS_2 bioFET device. The black line in each graph represents a topological cross-section of the image, whereas the blue line depicts the cross-sectional SP.

To optimize the immobilized PSA antibody concentration topologically, we performed SP analyses of PSA antibodies at five different concentrations: 1 pg/ml, 100 pg/ml, 10 ng/ml, 1 μg/ml, and 100 μg/ml (Figure 3). Remarkably, at 100 μg/ml, we could not distinguish a single molecule because of antibody aggregation, as shown in Figure 3(e). To precisely detect the SP of the antibody, we further conducted quantitative and statistical analyses of the SP at the same five antibody concentrations (Figures 3(f) and 3(g)). The average SP of each distinct PSA antibody is about 200 mV from 1 pg/ml to 1 μg/ml. On the other hand, the average SP is about 400 mV at 100 μg/ml, after the antibodies became aggregated. We also performed a t-test using the SP data from neighboring conditions, and the results are shown in Figure 3(g). In the t-test, all P-values were estimated to be much larger than 0.05 except between 1 μg/ml and 100 μg/ml. In other words, the SP at different concentrations is statistically identical for neighboring conditions except between 1 μg/ml and 100 μg/ml. According to these results, there exists a critical concentration for a proper distribution without aggregation when PSA antibodies are adsorbed on to a MoS_2 surface. Figure 3(h) reveals a consistent probability (SP_{total}/SP_{max}) trend of the SP of the adsorbed PSA antibodies with respect to concentrations from 1 pg/ml to 1 μg/ml, where SP_{total} is the surface potential of the total number of adsorbed single PSA antibodies on the MoS_2 bioFET surface, and SP_{max} is the surface potential when distinct PSA antibodies fully cover the MoS_2 bioFET surface. Therefore, the probability is approximately proportional to the antibody concentration except at 100 μg/ml, where at 100 μg/ml of antibody, the probability was calculated by the SP_{total} on the area of aggregated antibodies per the SP_{max}.

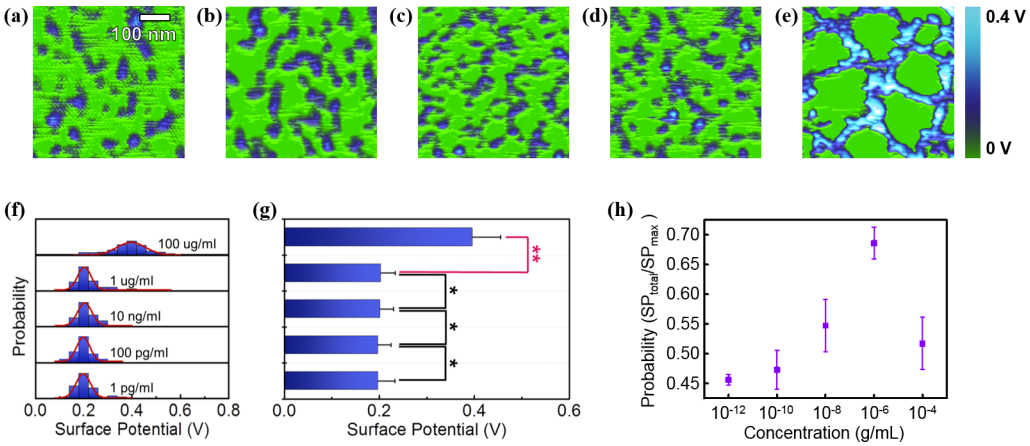

FIG. 3. ((a)–(e)) Surface potential map images observed by KFPM: (a) 1 pg/ml, (b) 100 pg/ml, (c) 10 ng/ml, (d) 1 μg/ml, and (e) 100 μg/ml of PSA antibody. (f) Histograms of the SP of different PSA antibody concentrations and their average values. (g) To confirm whether our approach can discriminate between two neighboring conditions, we performed t-tests between neighboring groups. P-values were calculated using the t-test (*P > 0.05, **P < 0.05). (h) Probability (SP_{total}/SP_{max}) of PSA antibodies with different antibody concentrations.

To study the correlation between the electrical performance of the MoS_2 bioFET and the SP generated by the adsorbed PSA antibodies, we measured the electrical sensor response of the MoS_2 bioFET with respect to the PSA antibody concentration, as shown in Figure 4(a). The I_d-V_{gs} curve for an as-fabricated MoS_2 bioFET without PSA antibody absorption indicates n-type behavior, where I_d and V_{gs} are the drain current flowing between S and D and the voltage applied to the Si gate, respectively, as described in Figures 1(b) and 1(d). The minimum drain current (I_{off}) lies in the negative V_{gs} regime. Upon increasing the applied PSA antibody concentration from 1 pg/ml to 1 μg/ml, the I_{off} for the MoS_2 bioFET increased. However, I_{off} decreased dramatically when the applied PSA antibody concentration was increased to 100 μg/ml. These results indicate that the electrical performance of the MoS_2 bioFET is unrelated to the high concentration (~100 μg/ml) of applied antibodies, which is similar to the previous SP analysis from KPFM. To examine these results more clearly, we constructed an off-current probability curve for the MoS_2 bioFET in the PSA antibody concentration range tested, where $I_{adsorbed}$ is the I_{off} at each treatment of the target biomolecules, and I_{max} is the highest current value at 1 μg/ml, as shown in Fig. 4(b). This trend is similar to the SP probability distribution (Figure 3(h)). More specifically, when the positively charged PSA antibody concentration ranged from 1 pg/ml to 1 μg/ml, the concentration of the adsorbed PSA antibody also increased, and all the PSA antibodies that can be distinguished at the single molecule level are well distributed on the MoS_2 surface (Figures 3(a)–3(d)), resulting in increased SP. This increased SP, generated by the positively charged PSA antibodies, is attributed

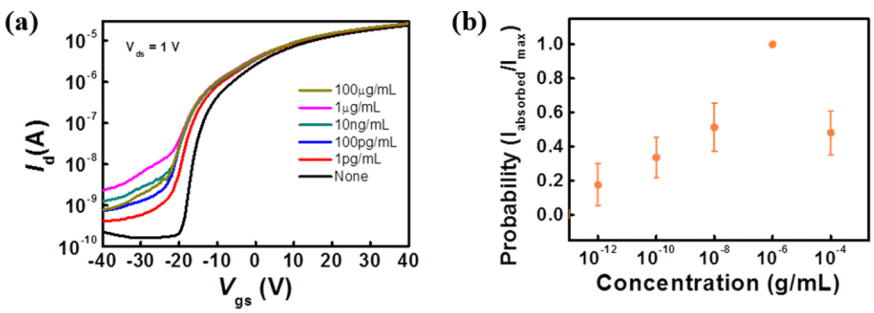

FIG. 4. (a) Transfer curves of the MoS_2 transistor under varying concentrations of PSA antibodies from 0 to 100 μg/ml. (b) The probability distribution showing the current response at different PSA antibody concentrations on MoS_2 biosensors (n = 5).

to an increase in electron concentration in a negative V_{gs} regime. As a result, the off-current of the MoS_2 bioFET gradually increased, as shown in Figure 4(a). On the other hand, at 100 μg/ml, the adsorbed PSA antibodies were no longer distinguishable at the single molecule level. As a result, the aggregated antibodies created a PSA antibody network (Figure 3(e)) that decreased the surface SP despite the high concentration (Figure 3(h)), resulting in the degradation of I_{off} in a negative V_{gs} regime. Hence, the electrical performance measured by the MoS_2 bioFET is strongly correlated to the SP of the MoS_2 surface, which is a function of the concentration and distribution patterns of the adsorbed PSA antibodies. Moreover, an optimized condition also exists for generating an electrical signal from the MoS_2 bioFET, which responds to the physically adsorbed PSA antibodies on the MoS_2 surface.

In conclusion, while varying the PSA antibody concentration, we examined the characteristics of physically adsorbed PSA antibodies on a MoS_2 bioFET surface using single-molecule imaging, and we also examined the SP using KPFM. In this characterization, we found that at a critical concentration, the adsorbed PSA antibodies aggregate and become a protein network. The SP decreased at the aggregate concentration, even though the number of PSA antibodies increased. Moreover, we measured the I_d-V_{gs} curves of the MoS_2 bioFET after the PSA antibodies were physically adsorbed on the bioFET surface using the same conditions as for the KPFM. This measurement is correlated with the SP values of the MoS_2 surface on which the PSA antibodies are adsorbed. The experimental results reveal that the electrical performance of a MoS_2 bioFET depends on both the antibody concentration and the distributed surface quality. Hence, an investigation of the optimal conditions for appropriate distribution of biological molecules on a MoS_2 surface is needed. This study provides insight into the local electrical properties of various bioFET devices and other electronic biosensors. Furthermore, the measurement of SP on a bioFET by KPFM analysis could be applied as a diagnostic tool to complement the electrical detection of a FET biosensor.

This work is partly supported by the U.S. National Science Foundation under Grant No. CMMI 826276, by the National Research Foundation of Korea (NRF) funded by the Ministry of Science, ICT, and Future Planning (Grant Nos. NRF-2014M3A9D7070732, NRF-2013M3C1A3059590, NRF-2015R1A1A1A05027488, NRF-2013R1A2A2A03005767, and NRF-2013R1A1A2053613), and by the Yonsei University Future-leading Research Initiative of 2015 (2015-22-0059). This research was partially supported by the Commercialization Promotion Agency for R&D Outcomes (COMPA) funded by the Ministry of Science, ICT, and Future Planning (MISP).

The authors have no competing financial interests to declare.

[1] G. Lee, K. Eom, J. Park, J. Yang, S. Haam, Y. M. Huh, J. K. Ryu, N. H. Kim, J. I. Yook, and S. W. Lee, Angew. Chem., Int. Ed. **51**(24), 5837 (2012).
[2] A. K. Sinensky and A. M. Belcher, Nat. Nanotechnol. **2**(10), 653 (2007).
[3] E. Stern, J. F. Klemic, D. A. Routenberg, P. N. Wyrembak, D. B. Turner-Evans, A. D. Hamilton, D. A. LaVan, T. M. Fahmy, and M. A. Reed, Nature **445**(7127), 519 (2007).
[4] E. Stern, A. Vacic, N. K. Rajan, J. M. Criscione, J. Park, B. R. Ilic, D. J. Mooney, M. A. Reed, and T. M. Fahmy, Nat. Nanotechnol. **5**(2), 138 (2010).
[5] F. Vollmer and S. Arnold, Nat. Methods **5**(7), 591 (2008).
[6] B. L. Allen, P. D. Kichambare, and A. Star, Adv. Mater. **19**(11), 1439 (2007).
[7] B. Kim, J. Lee, S. Namgung, J. Kim, J. Y. Park, M.-S. Lee, and S. Hong, Sens. Actuators B-Chem. **169**, 182 (2012).
[8] K. Maehashi, T. Katsura, K. Kerman, Y. Takamura, K. Matsumoto, and E. Tamiya, Anal. Chem. **79**(2), 782 (2007).
[9] X. Duan, Y. Li, N. K. Rajan, D. A. Routenberg, Y. Modis, and M. A. Reed, Nat. Nanotech. **7**(6), 401 (2012).
[10] A. Gao, N. Lu, P. Dai, T. Li, H. Pei, X. Gao, Y. Gong, Y. Wang, and C. Fan, Nano Lett. **11**(9), 3974 (2011).
[11] M. A. Bangar, D. J. Shirale, W. Chen, N. V. Myung, and A. Mulchandani, Anal. Chem. **81**(6), 2168 (2009).
[12] B. Kannan, D. E. Williams, C. Laslau, and J. Travas-Sejdic, Biosens. Bioelectron. **35**(1), 258 (2012).
[13] X. Chen, C. K. Wong, C. A. Yuan, and G. Zhang, Sens. Actuators B-Chem. **177**, 178 (2013).
[14] Y. Choi, T. J. Olsen, P. C. Sims, I. S. Moody, B. L. Corso, M. N. Dang, G. A. Weiss, and P. G. Collins, Nano Lett. **13**(2), 625 (2013).
[15] N. S. Ramgir, Y. Yang, and M. Zacharias, Small **6**(16), 1705 (2010).
[16] X. Zhao, B. Cai, Q. Tang, Y. Tong, and Y. Liu, Sensors **14**(8), 13999 (2014).
[17] J. Lee, P. Dak, Y. Lee, H. Park, W. Choi, M. A. Alam, and S. Kim, Sci. Rep. **4**, 7352 (2014).
[18] Y. Zuo, L. Wu, K. Cai, T. Li, W. Yin, D. Li, N. Li, J. Liu, and H. Han, ACS Appl. Mater. Interfaces **7**(32), 17725 (2015).
[19] Y. Huang, X. Dong, Y. Liu, L.-J. Li, and P. Chen, J. Mater. Chem. **21**(33), 12358 (2011).
[20] Y. Huang, X. Dong, Y. Shi, C. M. Li, L.-J. Li, and P. Chen, Nanoscale **2**(8), 1485 (2010).
[21] M. Chhowalla, H. S. Shin, G. Eda, L.-J. Li, K. P. Loh, and H. Zhang, Nat. Chem. **5**(4), 263 (2013).
[22] H. Wang, L. Yu, Y.-H. Lee, Y. Shi, A. Hsu, M. L. Chin, L.-J. Li, M. Dubey, J. Kong, and T. Palacios, Nano Lett. **12**(9), 4674 (2012).

[23] D. Sarkar, W. Liu, X. Xie, A. C. Anselmo, S. Mitragotri, and K. Banerjee, ACS Nano **8**(4), 3992 (2014).
[24] L. Wang, Y. Wang, J. I. Wong, T. Palacios, J. Kong, and H. Y. Yang, Small **10**(6), 1101 (2014).
[25] H. Lee, S. W. Lee, G. Lee, W. Lee, J. H. Lee, K. S. Hwang, J. Yang, S. W. Lee, and D. S. Yoon, Nanoscale **8**, 13537 (2016).
[26] C. Park, K. Jang, S. Lee, J. You, S. Lee, H. Ha, K. Yun, J. Kim, H. Lee, and J. Park, Nanotechnology **26**(30), 305501 (2015).
[27] S. Sadewasser, P. Jelinek, C.-K. Fang, O. Custance, Y. Yamada, Y. Sugimoto, M. Abe, and S. Morita, Phys. Rev. Lett. **103**(26), 266103 (2009).
[28] T. Kwon, J. Park, G. Lee, K. Nam, Y.-M. Huh, S.-W. Lee, J. Yang, C. Y. Lee, and K. Eom, J. Phys. Chem. Lett. **4**(7), 1126 (2013).
[29] V. Panchal, R. Pearce, R. Yakimova, A. Tzalenchuk, and O. Kazakova, Sci. Rep. **3**, 2597 (2013).
[30] K. Nam, K. Eom, J. Yang, J. Park, G. Lee, K. Jang, H. Lee, S. W. Lee, D. S. Yoon, C. Y. Lee, and T. Kwon, J. Mater. Chem. **22**(44), 23348 (2012).
[31] E. Koren, Y. Rosenwaks, J. Allen, E. Hemesath, and L. Lauhon, Appl. Phys. Lett. **95**(9), 092105 (2009).
[32] G. Lee, W. Lee, H. Lee, S. Woo Lee, D. Sung Yoon, K. Eom, and T. Kwon, Appl. Phys. Lett. **101**(4), 043703 (2012).
[33] H. Lee, W. Lee, J. H. Lee, and D. S. Yoon, J. Nanomater. **2016**, 21.
[34] W. Lee, H. Jung, M. Son, H. Lee, T. J. Kwak, G. Lee, C. H. Kim, S. W. Lee, and D. S. Yoon, RSC Adv. **4**(100), 56561 (2014).
[35] J. Park, J. Yang, G. Lee, C. Y. Lee, S. Na, S. W. Lee, S. Haam, Y.-M. Huh, D. S. Yoon, K. Eom, and T. Kwon, ACS Nano **5**(9), 6981 (2011).
[36] C. Dean, A. Young, I. Meric, C. Lee, L. Wang, S. Sorgenfrei, K. Watanabe, T. Taniguchi, P. Kim, and K. Shepard, Nat. Nanotechnol. **5**(10), 722 (2010).
[37] S.-P. Lin, T.-Y. Chi, T.-Y. Lai, and M.-C. Liu, Sensors **12**(12), 16867 (2012).